Supporting Information

for

Contrasting effects of rainfall on permafrost degradation within the desertified regions of the Tibetan Plateau

Luyang Wang [1, 2], Ziteng Fu [1, 2], Dongliang Luo [1, 3], Guanli Jiang [1, 3], Wenxin Zhang [4], Zhongqiong Zhang [1, 3], Yuzhong Yang [1, 3], Siru Gao [1], Wenyan Du [1, 3], and Qingbai Wu [1, 2, 3] ✉

[1] State Key Laboratory of Cryospheric Science and Frozen Soil Engineering, Northwest Institute of Eco-Environment and Resources, Chinese Academy of Sciences, Lanzhou 730000, China. [2] Qinghai-Beiluhe Plateau Frozen Soil Engineering Safety National Observation and Research Station, Chinese Academy of Sciences, Lanzhou, 730000, China. [3] University of Chinese Academy of Sciences, Beijing 100049, China. [4] School of Geographical and Earth Sciences, University of Glasgow, Glasgow, G12 8QQ, Scotland, UK. ✉e-mail: **qbwu@lzb.ac.cn**

This PDF file includes:

Figure S1 to S7

Supporting text SI. 1

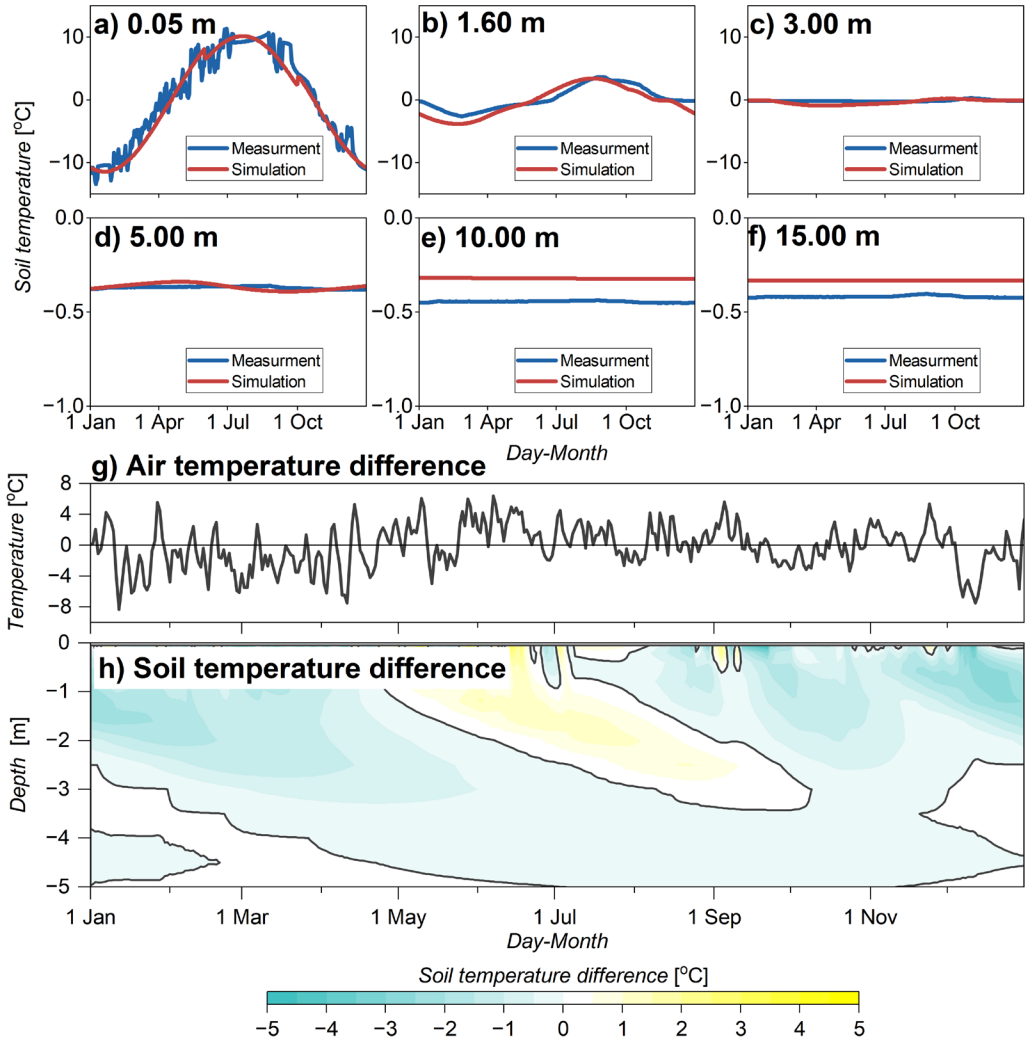

Fig. S1 | (a-f) Measured and simulated soil temperature time series. (g) Differences between the smoothed air temperature and the measured air temperature. (h) Differences between simulated and measured isotherms.

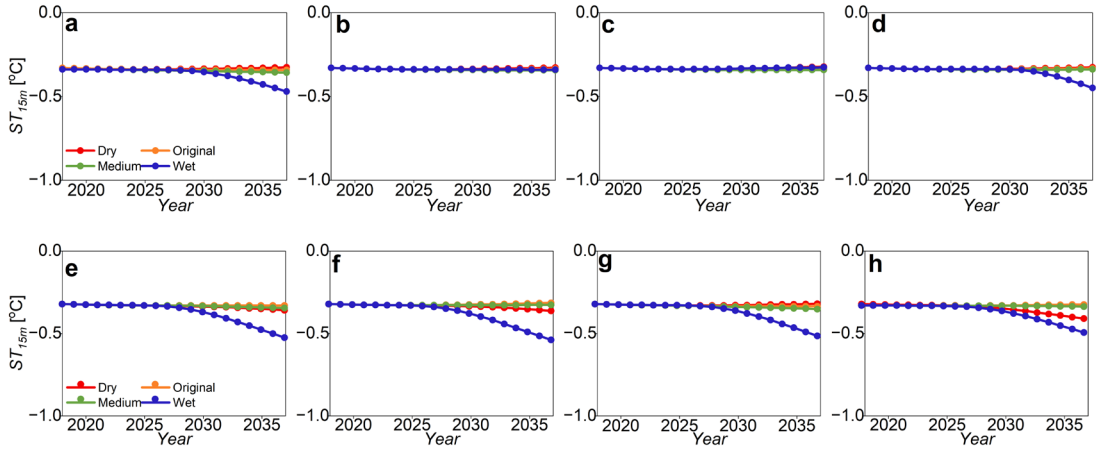

Fig. S2 | ST_{15m} under different SR and ER scenarios. Sub-figures a to d represent the standard SR scenarios, the early-summer 50% SR scenarios, the mid-summer 50% SR scenarios, and late-summer 50% SR scenarios, respectively. Suib-figures e to h represent the standard ER scenarios, the 150% ER scenarios, the 50% ER scenarios, and the 4-consecutive-year ER scenarios, respectively.

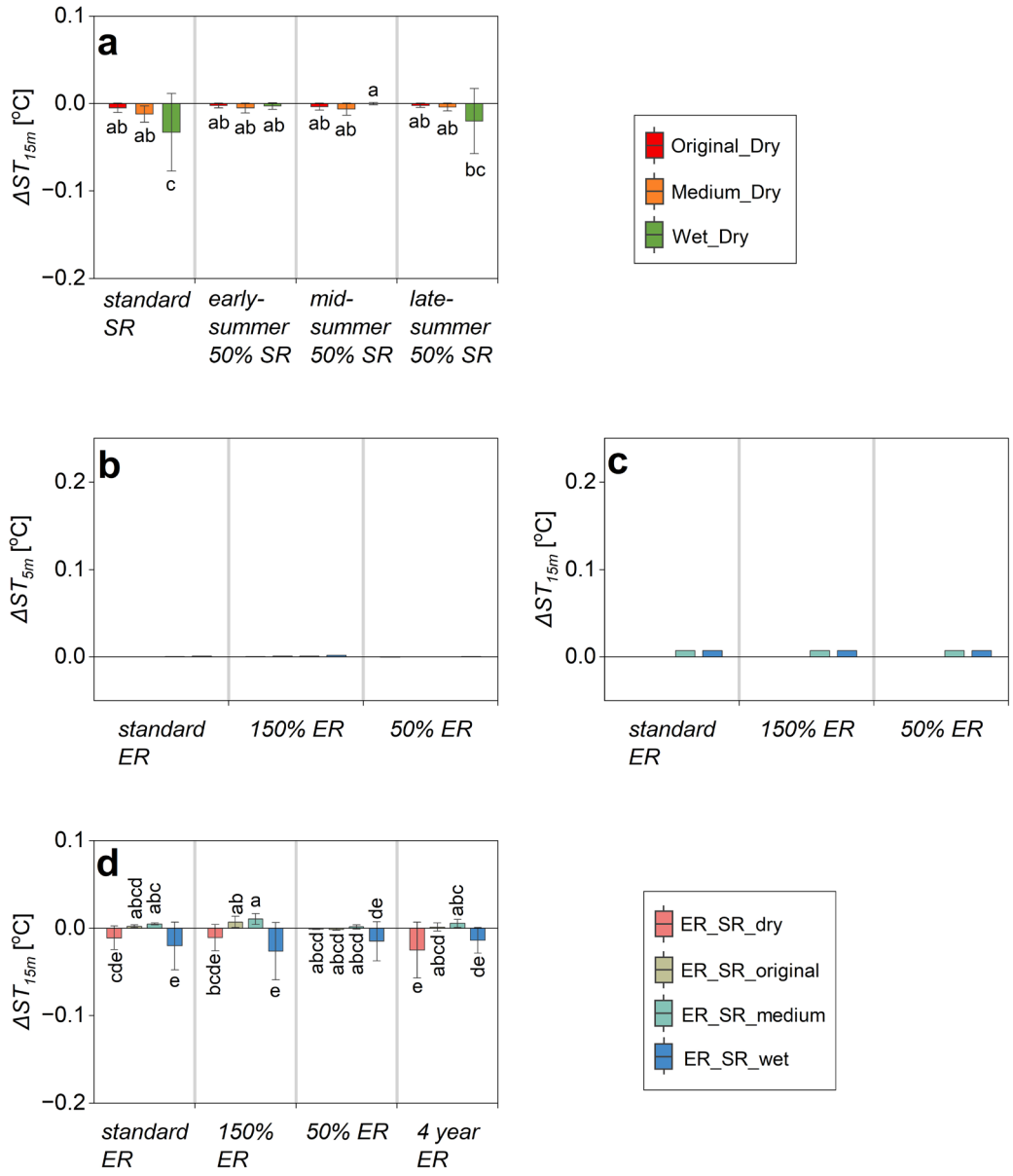

Fig. S3 | Statistical differences of ST_{5m} and ST_{15m} under different SR and ER scenarios. (a) Statistical differences of ST_{15m} under different SR scenarios. Statistical short-term differences of ST_{5m} (b) and ST_{15m} (c) under different ER scenarios. Statistical long-term differences ST_{15m} (d) under different ER scenarios. Bars represent the mean values and whiskers denote ± 1.5 SD. The letters indicate statistically significant differences at the $p<0.05$ level.

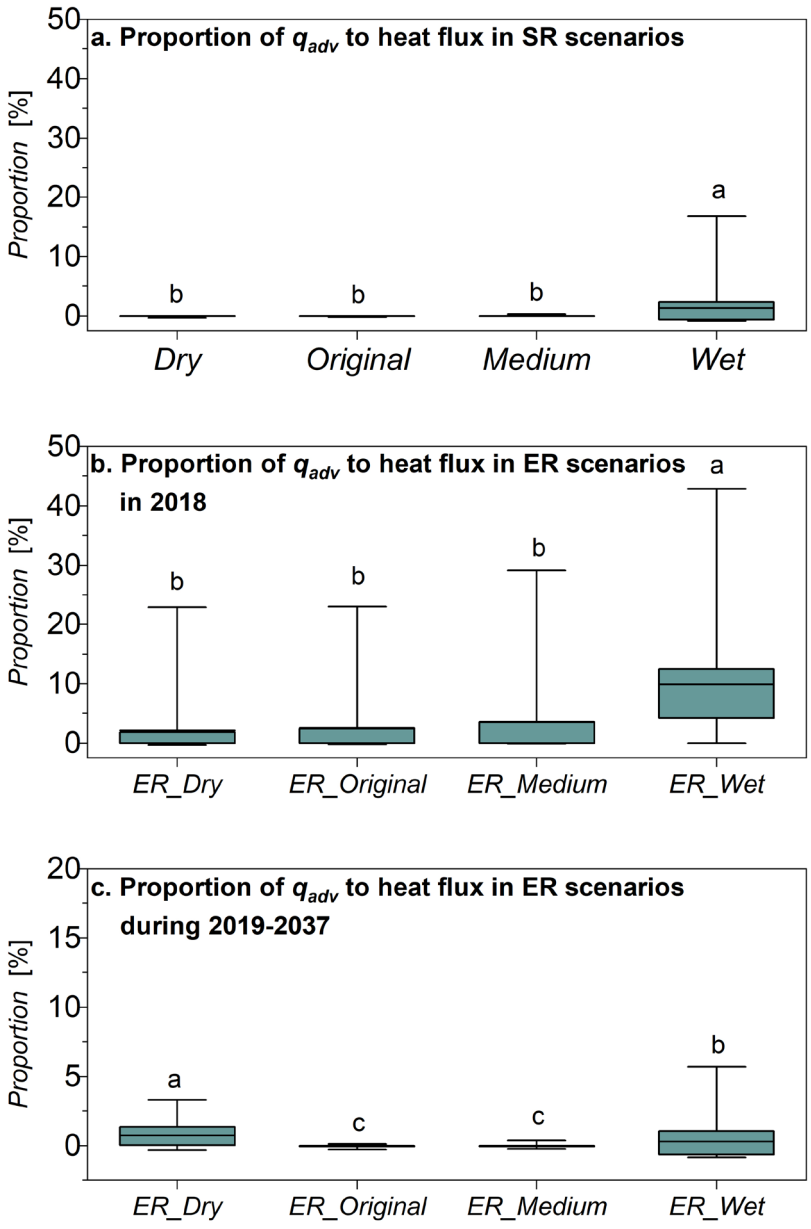

Fig. S4 | Proportion of advective heat flux to total heat flux of active layer under the standard SR scenarios (a), the standard ER scenarios in 2018 (b), and the standard ER scenarios during 2019-2037 (c). The statistical data are derived from June to September during 2018-2037, in 2018, and during 2019-2037 in sub-figure a, b, and c, respectively. Box plots illustrate the quartile range, with whiskers extending to the minimum and maximum values, and a bold horizontal line represents the mean value. The letters above the box plots indicate statistically significant differences at the $p<0.05$ level.

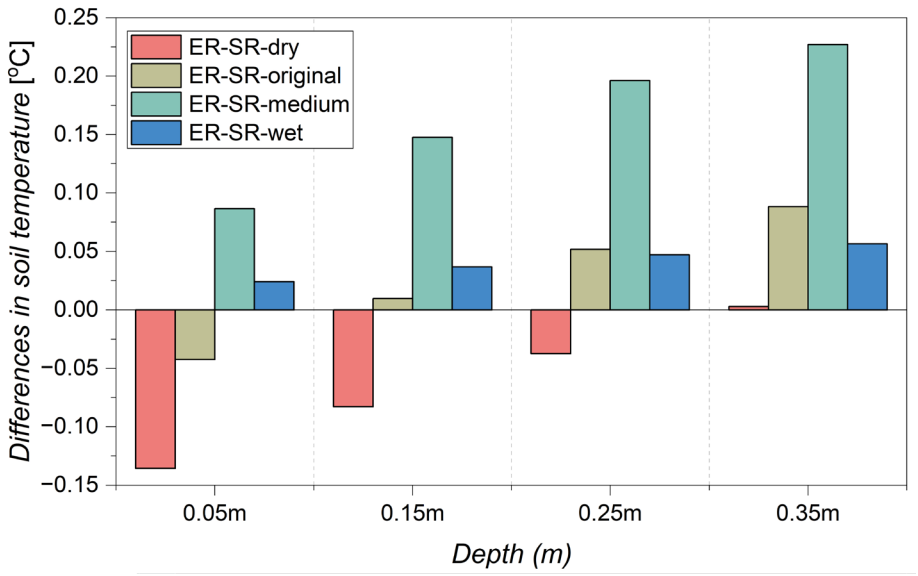

Fig. S5 | ER-induced changes in mean annual soil temperature at different shallow depths in 2018.

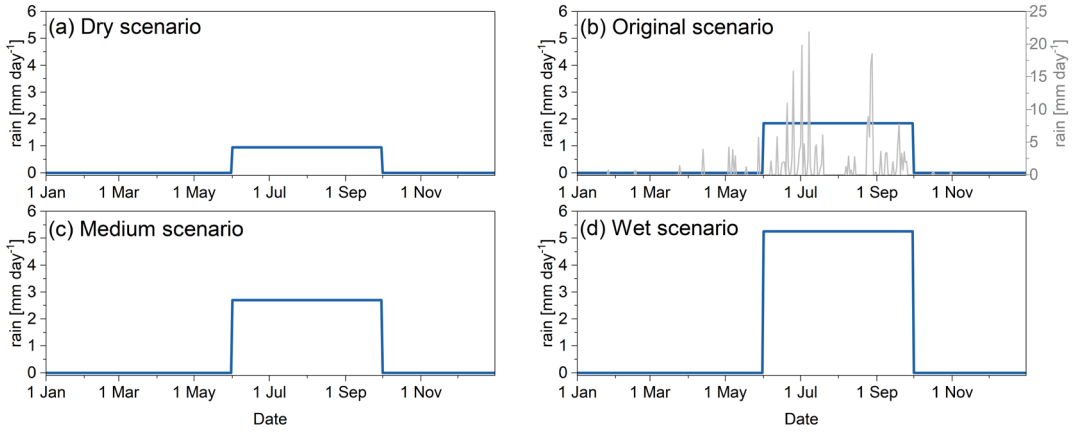

Fig. S6 | Temporal distribution patterns of summer rainfall in the standard SR scenarios

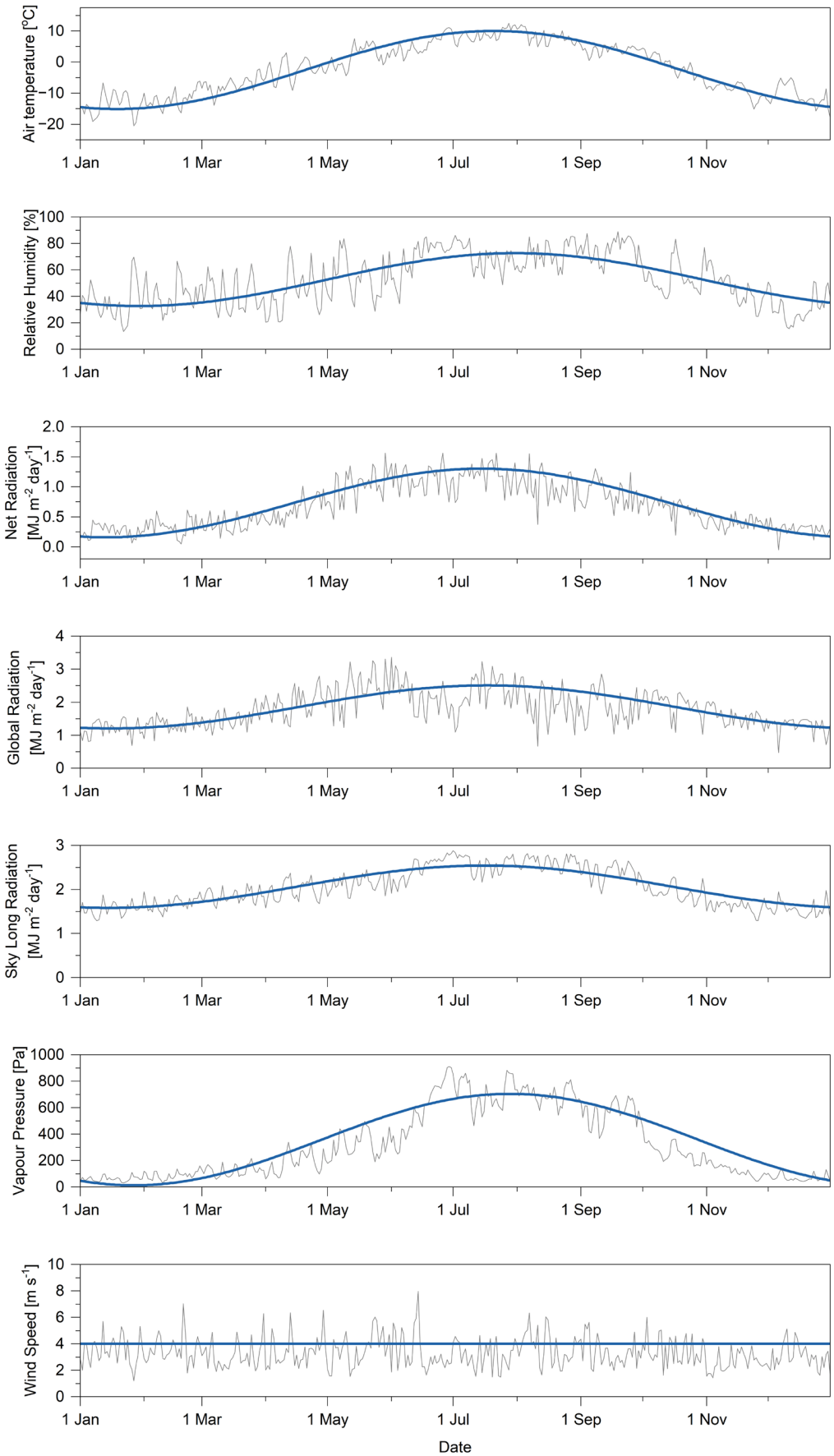

Fig. S7 | Smoothed meteorological data

SI.1 Variations in surface energy balance components with SR increasing and ER

Increasing SR substantially raises the TWC of topsoil (Fig. S8a), which lowers surface albedo and then increases net shortwave radiation (Fig. S8b and c). Meanwhile, increasing SR intensifies evaporation (Fig. S8d), leading to an increase in latent heat flux and a decline in ground surface temperature (Fig. S8e and f). The decline in ground surface temperature not only reduces sensible heat flux (Fig. S6i) but also decreases outgoing surface longwave radiation (Fig. S8g and i). The decrease in outgoing surface longwave radiation leads to an increase in net longwave radiation because the atmospheric longwave radiation remains a fixed input in the model setting (Fig. S8h). The increases in net shortwave radiation and net longwave radiation cause an increase in net radiation (Fig. S8j). Finally, the magnitudes of SR-induced variations in latent heat flux, sensible heat flux, and net radiation are different, and their combined effect is a persistent decline in q_s, indicating that increasing SR markedly reduces the external heat input into the ground.

In the year when ER occurs, ER can enhance topsoil wetting and evaporation, and accordingly decreases sensible heat flux, increases latent heat flux, and raises net radiation, and moreover, the strength of these changes is strongly modulated by SR. As SR increases, the ER-induced increase in TWC of topsoil is enhanced (Fig. S9a), and the decline in albedo is also boosted (Fig. S9b). It should be emphasized, however, that even without extreme rainfall, the Wet scenario already can lead to a substantial increase in TWC of topsoil because of the high rainfall amount of this scenario (Fig. S10d). Consequently, the topsoil wetting effect of ER in the Wet scenario is quite limited (Fig. S10d). This explains why the changes in topsoil TWC and albedo in the ER_Wet scenario are quite small (Fig. S9a, b), producing almost no change in net shortwave radiation (Fig. S9c). Overall, ER enhances evaporation, but the magnitude of this enhancement declines with increasing SR (Fig. S9d). As a result, the increase in latent heat flux also weakens (Fig. S9e), ultimately reducing the magnitude of surface temperature dropping (Fig. S9f). This further reduces the ER-induced increase in net

longwave radiation and the ER-induced decreases in sensible heat flux and net radiation (Fig. S9h–j). Ultimately, ER decreases q_s in the year of ER occurrence, and the magnitude of this decrease progressively diminishes with increasing SR, and even shifts to a slight increase in the ER_Wet scenario. These results indicate that ER generally reduces external heat input into the ground, but this cooling effect weakens as SR increases and shifts to slight warming under wet conditions.

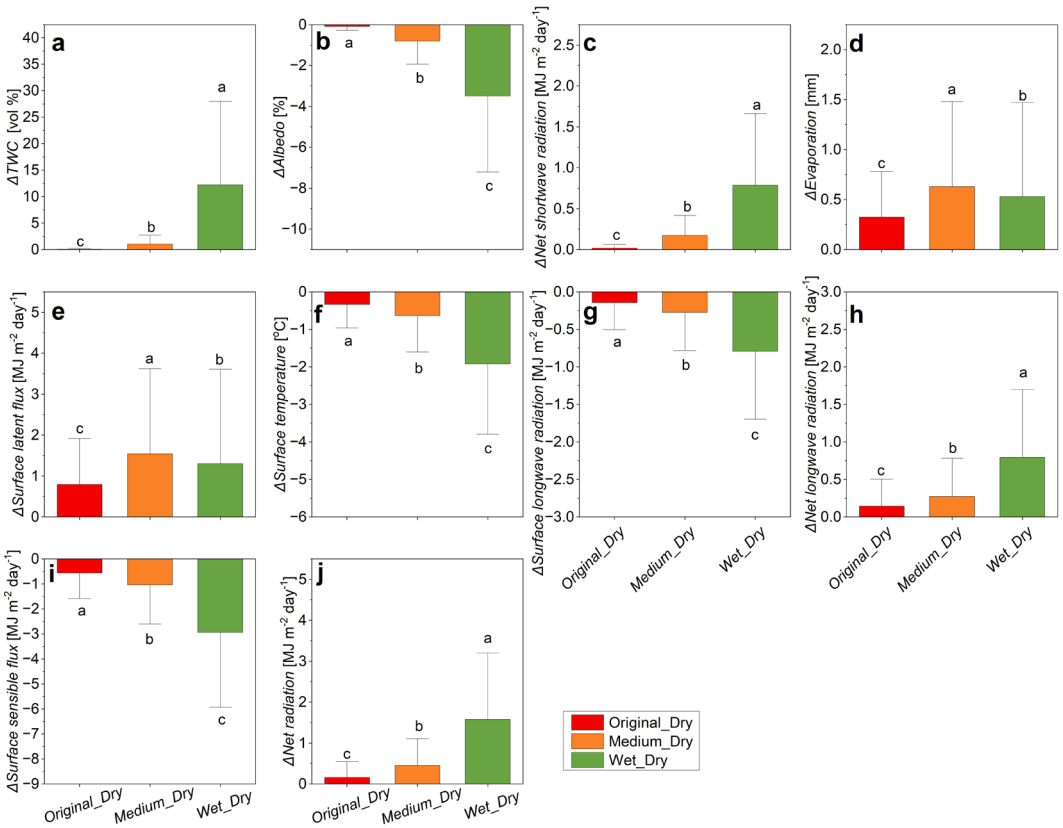

Fig. S8 | Statistical differences in components of surface energy balance between different standard SR scenarios. Statistical differences in TWC (a), albedo (b), net shortwave radiation (c), evaporation (d), surface latent flux (e), round surface temperature (f), surface longwave radiation (g), net longwave radiation (h), surface sensible flux (i), and net radiation (j). The bars represent mean values, with whiskers extending to ±1.5 SD. The letters above the box plots indicate statistically significant differences at the $p<0.05$ level.

In the years after ER occurs, the topsoil wetting effect caused by ER in the year of occurrence was enhanced by SR increasing, but this simultaneously constrains any further topsoil wetting in years after ER occurs. Accordingly, the increases in topsoil TWC in later years remains evident only in the ER_dry scenario, whereas it is weak in the other ER scenarios (Fig. S11a). This further causes the changes in surface energy balance—including albedo reducing, surface temperature dropping, sensible heat flux

decreasing, and net radiation increasing—to be significantly only in the ER_dry scenario (Fig. S11b–j). As a consequence, q_s declines significantly only under the ER_dry scenario, while little change is observed in the other ER scenarios. These results indicate that the long-term cooling effect of ER occurs mainly under dry condition, but is substantially weakened or nearly disappears under wetter conditions.

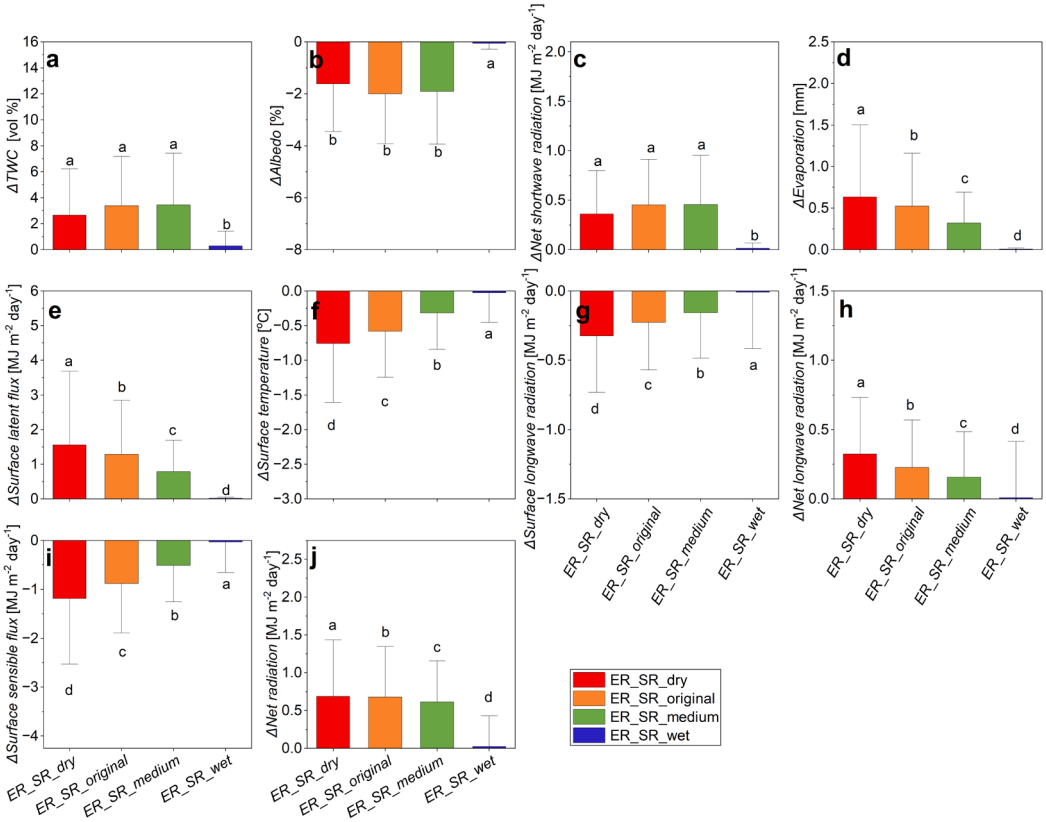

Fig. S9 | Statistical differences in components of surface energy balance between different standard ER scenarios in 2018. Statistical differences in TWC (a), albedo (b), net shortwave radiation (c), evaporation (d), surface latent flux (e), round surface temperature (f), surface longwave radiation (g), net longwave radiation (h), surface sensible flux (i), and net radiation (j). The bars represent mean values, with whiskers extending to ±1.5 SD. The letters above the box plots indicate statistically significant differences at the $p<0.05$ level.

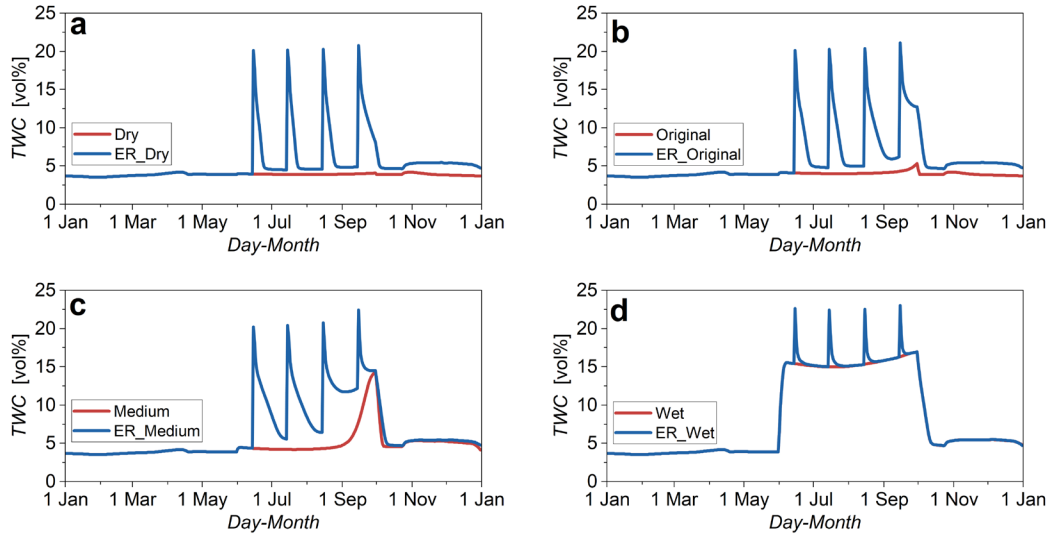

Fig. S10 | Comparison of surface TWC in 2018 between the SR scenario and the corresponding ER scenario.

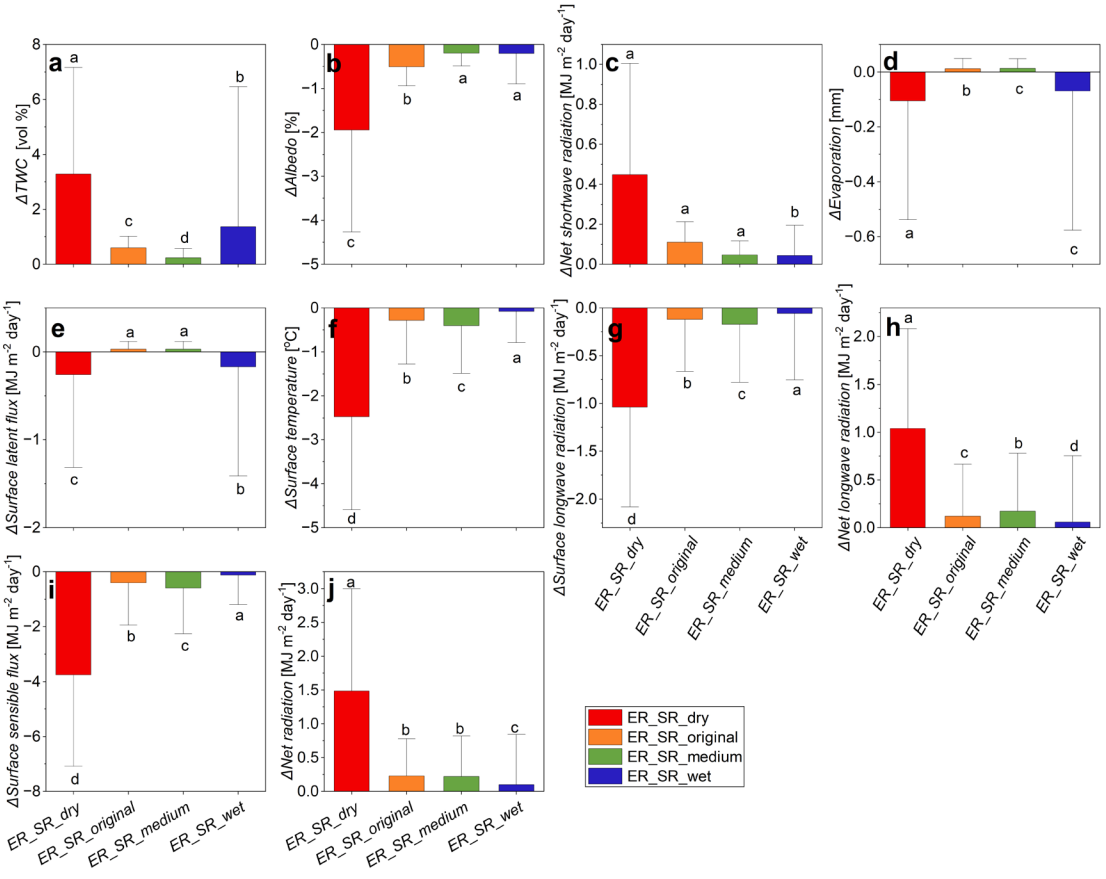

Fig. S11 | Statistical differences in components of surface energy balance between different standard ER scenarios during 2019-2037. Statistical differences in TWC (a), albedo (b), net shortwave radiation (c), evaporation (d), surface latent flux (e), round surface temperature (f), surface longwave radiation (g), net longwave radiation (h), surface sensible flux (i), and net radiation (j). The bars represent mean values, with whiskers extending to ±1.5 SD. The letters above the box plots indicate statistically significant differences at the $p<0.05$ level.